Point Mean Beam Length, a New Concept to Enhance the Computational Efficiency of Multi-Dimensional, Non-Gray Radiative Heat Transfer

By

Walter W. Yuen
Department of Mechanical Engineering
Santa Clara University
500 El Camino Real
Santa Barbara, California, 95053
Tel: 805-403-3637
Email: wwyuen@scu.edu

Wai Cheong Tam
Fire Research Division
100 Bureau Drive
National Institute of Standards and Technology
Gaithersburg, Maryland, USA
Tel: 301-975-8202
Email: waicheong.tam@nist.gov

Abstract

A new concept of point mean beam length (PMBL) is introduced. For enclosures with simple geometry, this concept provides a fundamental self-consistent interpretation on the various different definition of the conventional mean beam length. The concept is further demonstrated to be effective in enhancing the computational efficiency for multi-dimensional radiative heat transfer in non-gray media. In the evaluation of radiative exchange between two perpendicular areas with a common edge, the use of PMBL leads to a factor of 100 to 400 reduction in computational effort compared to the direct integration approach. For practical applications, PMBL is combined with RADNNET (a neural network correlation for a one-dimensional CO_2/H_2O/soot combustion mixture) to generate two highly efficient and accurate solvers for the evaluation of exchange factors between two parallel or perpendicular rectangular areas of arbitrary dimensions with an intervening combustion mixture.

Nomenclature

a, a_λ	absorption coefficient
A_i	area (i = 1,2)
dA_i	differential area (i = 1,2)
$ds_1 s_2$	differential exchange factor between differential area dA_1 and finite area A_2
D_x	dimensional variables, Fig. 1a, 1b
D_y	dimensional variables, Fig. 1a, 1b
D_z	dimensional variables, Fig. 1a, 1b

E_3	exponential integral function
E	error using a constant length scale to approximate the transmissivity between dA_1 and A_2, Eq. (10b)
f_v	soot volume fraction
F_{d1-2}	differential view factor between differential area dA_1 and finite area A_2
F_{1-2}	differential view factor between finite area A_1 and finite area A_2
L	pathlength
L_{pmb}	point mean beam length
$L_{pmb,av}$	average point mean beam length
L_{mb}	conventional mean beam length
L_{opmb}	optimal point mean beam length
$s_1 s_2$	exchange factor between finite area A_1 and finite area A_2
p_{H_2O}	partial pressure of H_2O
S	error function used to determine the average PMBL, Eq. (10a)
X_1	dimensional variable, Figs. (10a) and (10b)
X_2	dimensional variable, Figs. (10a)
Y_1	dimensional variable, Figs. (10a) and (10b)
Y_2	dimensional variable, Figs. (10a) and (10b)
Z_2	dimensional variable, Fig. (10b)
ΔX	dimensional variable, Figs. (10a) and (10b)
ΔY	dimensional variable, Figs. (10a) and (10b)
ΔZ	dimensional variable, Figs. (10a) and (10b)

Greek Symbol

ζ_x	dimensionless variable, Eqs. (8) and (9)
ζ_y	dimensionless variable, Eqs. (8) and (9)
η_y	dimensionless variable, Eq. (12) and (13)
η_z	dimensionless variable, Eq. (12) and (13)
θ_1	angular variable, Eq. (1)
θ_2	angular variable, Eq. (1)
τ_g	one-dimensional transmissivity of a gas mixture, Eq. (16)
τ_{d1-2}	transmissivity between area dA_1 and A_2, Eq. (2)

1. Introduction

The concept of mean beam length (MBL) was introduced many years ago by Hottel and other researchers [1-3] as a practical tool to estimate the effect of radiative heat transfer in a multi-dimensional non-gray system. Since most, if not all, of the spectroscopic gaseous emission data were generated from one-dimensional line-of-sight measurements, there was a need to justify the application of the data to practical combustion systems that are generally multi-dimensional. Since direct integrations over wavelength and geometry are too complicated to carry out (particularly in the 1960's, 70's and 80's with the lack of computational power), much research were directed toward the development of an

effective length scale (identified with the name mean beam length, MBL, by Hottel [1]) for combustors with different geometry and gases with different absorption bands [4-9]. The success of such efforts, however, were limited as MBL was found to be different for combustors with different geometries. Due to its spectral dependence, MBL was also different for different absorption band with different optical thicknesses. Currently, for an entire uniform isothermal medium radiating to its entire boundary, the recommended approach is to assume that MBL is the product of the optically thin limiting expression of MBL (which can be shown to be equal to $4V/A$ with V being the volume and A the bounding area of an enclosure) and a "correction factor" (recommended to be 0.9 Hottel and his co-workers [1]). But with little theoretical justification, this approach is generally considered to be "approximate" and "qualitative" by the practical engineering community. Safety factors are typically required to compensate for these uncertainties in engineering designs. This recommended approach is also limited in its application since it can only evaluate the average radiative heat transfer to the entire boundary. There are currently no recommended approach to determine the distribution of the heat transfer to its boundary from an entire uniform isothermal medium other than by direct numerical integration.

The interest in MBL has decreased significantly over recent years. Due to the increase in computational power, the focus of the radiation research community is more on development of effective computational schemes. While efforts were made to integrate the MBL concept into the zonal method [11, 12], the success is somewhat limited due to the complex dependence of MBL on geometry and mixture properties. But even with the increased computational power and the significant amount of research on computational method over the past ten years, direct numerical computation of the radiative heat flux in a 3-D enclosure is currently still too complex and time consuming for a homogenous non-gray medium [13]. The radiation solver in all of the existing heat transfer codes (e.g. CFAST [14], FDS [15], FLUENT) continues to use approximation methods to deal with the non-gray multi-dimensional radiative effects without much validation. Fundamentally, there is still an urgent need for a validated computational approach which can account for the non-gray multi-dimensional effect of radiative heat transfer accurately and efficiently.

In the present work, a new concept of point mean beam length (PMBL) is introduced. In contrast to the traditional concept of MBL which is defined for radiative exchange between two finite areas or between a volume and its total surrounding surface, PMBL is defined for radiation emitted from a differential area (at a point in a finite area), transmitted to and absorbed by a second finite area. Numerical data show that while PMBL is still a function of absorption coefficient of the intervening medium similar to the traditional MBL, its dependence is not strong for a given geometrical configuration. A constant length scale, the "optimal" PMBL(OPMBL), can be used to predict accurately the spectral transmission between the differential area and the second finite area over the entire range of the absorption coefficient. The 1-D total integrated absorption or transmission model can thus be used with one length scale (OPMBL) to predict the multi-dimensional absorption and transmission. For an enclosure with symmetric geometrical configuration such as a sphere, PMBL is identical to the conventional MBL and its value is demonstrated to be consistent with the various conventional MBL's defined for the different limiting expressions of gas band absorptance. In fact, OPMBL gives a theoretical justification of the "correction factor" used in the conventional MBL approach. For numerical computation, OPMBL reduces the evaluation of radiative exchange between two surfaces

to a single area integration over the emitting area, which can be done accurately and efficiently. As illustrations, two fast and accurate radiation solvers for the evaluation of radiative heat transfer between two parallel or perpendicular rectangular surfaces with arbitrary dimensions are developed and made available to the engineering community.

2. The concept of point mean beam length (PMBL)

For a diffusely emitting area dA_1 and a second finite area A_2, the differential exchange factor is given by

$$ds_1 s_2 = dA_1 \int_{A_2} \frac{cos\theta_1 cos\theta_2}{\pi L^2} e^{-aL} dA_2 \tag{1}$$

where θ_i $(i = 1,2)$ is the angle between the unit surface normal at the two differential surface dA_i *(i = 1, 2)* and the line of sight between the two differential surfaces. L is the length of the line of sight and a is the absorption coefficient of the intervening medium. A point mean beam length, L_{pmb} is defined to be the equivalent length such that the transmissivity between the two surfaces can be written as

$$\tau_{d1-2} = \frac{ds_1 s_2}{dA_1 F_{d1-2}} = e^{-aL_{pmb}} \tag{2}$$

where the differential view factor, F_{d1-2}, defined by

$$F_{d1-2} = \int_{A_2} \frac{cos\theta_1 cos\theta_2}{\pi L^2} dA_2 \tag{3}$$

Equation (1) can be integrated over area A_1 to yield to the total exchange factor

$$s_1 s_2 = \int_{A_1} \int_{A_2} \frac{cos\theta_1 cos\theta_2}{\pi L^2} e^{-aL} dA_2 \, dA_1 \tag{4}$$

The conventional mean beam length, MBL, for the two areas A_1 and A_2 is defined as

$$\tau_{1-2} = \frac{s_1 s_2}{A_1 F_{1-2}} = e^{-aL_{mb}} \tag{5}$$

with F_{1-2} being the view factor between the two finite areas, A_1 and A_2 given by

$$F_{1-2} = \int_{A_1} \int_{A_2} \frac{cos\theta_1 cos\theta_2}{\pi L^2} dA_2 dA_1$$

A comparison between Eqns. (2) and (5) yields the following relation between PMBL and MBL,

$$e^{-aL_{mb}} = \frac{1}{A_1 F_{1-2}} \int_{A_2} F_{d1-2} e^{-aL_{pmb}} dA_2 \tag{6}$$

It should be noted that for a general enclosure, PMBL is defined for a local differential area and is not the same as MBL. But for enclosure with geometrical symmetry such a sphere, infinite cylinder and slab, PMBL is identical at every point of the emitting surface. PMBL is thus identical to the conventional MBL for such enclosures.

To illustrate the mathematical behavior of PMBL, a spherical enclosure is considered. This geometry is selected because the conventional MBL for sphere has been studied extensively by many investigators [2,4] using different expressions of gas absorption band. The relationship between PMBL and the conventional MBL concepts can thus be formally established. Using the coordinate system as shown on Figure 1, Eq. (1) becomes

$$ds_1 ds_2 = \frac{R^2(1+cos\theta)^2}{\pi L^4} e^{-aL} dA_1 dA_2 \tag{7}$$

Consider A_2 as the entire spherical surface, Eq. (7) can be integrated over the spherical surface to yield (a similar expression was also derived in reference [3])

$$\frac{ds_1 s_2}{dA_1} = -\frac{1}{aR} e^{-2aR} + \frac{1}{2(aR)^2}(1 - e^{-2aR}) \tag{8}$$

The PMBL is given by

$$\frac{L_{pmb}}{R} = -\frac{1}{aR} ln\left[-\frac{1}{aR} e^{-2aR} + \frac{1}{2(aR)^2}(1 - e^{-2aR})\right] \tag{9}$$

To determine OPMBL, an error function, *S(L)*, between the actual exchange factor and the approximate value generated by a constatn length scale, *L*, is introduced as follow

$$S(L) = \int_0^{(aR)_{0.01}} E(L)^2 \, d(aR) \tag{10a}$$

with

$$E(L) = \left|\frac{ds_1 s_2}{dA_1} - F_{d1-2} e^{-aR\frac{L}{R}}\right| \tag{10b}$$

The upper limit of the integration in Eq. (10a) is taken to be the point at which the transmissivity is 0.01 because both the approximate and exact expression of the transmissivity is close to zero and the error is insigficant. The PMBL for different optical thickness, *aR*, is shown in Figure 2. The numerical value of OPMBL, established by the minization of *S(L)* is shown in the same figure to be

$$\frac{L_{opmb}}{R} = 1.168 \tag{11}$$

To demonstrate the effectivenss of OPMBL, a comparison between the exact exchange factor (Eq. 8) and the approximate exchange factor generated by L_{opmb} ($e^{-aL_{opmb}}$) is shown in Figure 3. The agreement is excellent with a maximum absolute error of less than 0.03 . In general, the error is higher in the region with large optical thickness (aR > 3).

But this discrepancy is not important practically as the transmissivity is small (<0.05). In previous studies [2,4], the MBL for a weakly absorbing band was established to be $4R/3$, which is the optically thin limit of L_{pmb}, as shown in Figure 3. The MBL for a strongly absorbing band (the squre-root limit) was determined to be *6R/5*, which is consistent with Eq. (11). It is interesting to note that L_{opmb} is nearly identical to $0.9L_{mb,0}$, which is the empirical MBL relation currently recommended for usage over all optical thickness.

Numerical studies show that the concept of OPMBL is an effective representation of MBL for other geometrical configurations such as infinite cylinders, parallel slab and general two-dimensiional systems. A detailed presentation of these results is quite extensive and will be presented in a separate publication. For the remainder of this paper, the focus will be on the development of OPMBL for two specific three-dimensional geometries and to demonstrate how the PMBL concept can enhance the computational efficiency of general three-dimensional non-gray radiative heat transfer.

3. PMBL for two fundamental three-dimensional configurations

The two fundamental three-dimensional configurations are shown in Figs. (4a) and (4b). In both cases, dA_1 is a differential area at the origin with a unit normal in the z direction. In Fig. (4a), A_2 is a rectangular area parallel to dA_1 with a dimension $D_x \times D_y$ at the plane $z = D_z$. After some mathematical manipulation (detail given in Appendix A), it can be shown that the PMBL is reduced to a semi-analytical expression as follow

$$\frac{L_{pmb}}{D_z} = -\frac{1}{aD_z} ln \left\{ \frac{1}{F_{d1-2}} \left[\frac{1}{2} \left[E_3(aD_z) - \left(\frac{1}{\sqrt{\zeta_y^2+1}} \right)^2 E_3\left(aD_z\sqrt{\zeta_y^2+1}\right) \right] - \frac{1}{\pi} \int_{\zeta_x}^{\sqrt{\zeta_x^2+\zeta_y^2}} arcos\left(\frac{\zeta_x}{s}\right) \frac{e^{-aD_z\sqrt{1+s^2}}}{(1+s^2)^2} sds + \frac{1}{\pi} \int_{\zeta_y}^{\sqrt{\zeta_x^2+\zeta_y^2}} arsin\left(\frac{\zeta_y}{s}\right) \frac{e^{-aD_z\sqrt{1+s^2}}}{(1+s^2)^2} sds \right] \right\} \qquad (12)$$

with $\zeta_x = \frac{D_x}{D_z}$, $\zeta_y = \frac{D_y}{D_z}$ and $E_3(x)$ being the third exponential integral function. F_{d1-2} is the view factor given by

$$F_{d1-2} = \frac{1}{2\pi} \left\{ \frac{\zeta_x}{(1+\zeta_x^2)^{1/2}} tan^{-1}\left[\frac{\zeta_y}{(1+\zeta_x^2)^{1/2}}\right] + \frac{\zeta_y}{(1+\zeta_y^2)^{1/2}} tan^{-1}\left[\frac{\zeta_x}{(1+\zeta_y^2)^{1/2}}\right] \right\} \qquad (13)$$

The spectral behavior of L_{pmb} is illustrated in Figure 5, in which L_{pmb} for a square area A_2 ($D_x = D_y$) of different size (D_x/D_z) are plotted against the optical thickness aD_z. For each goemetric configuraton, an OPMBL is evaluated and is shown as a point along the PMBL curve. As expected, L_{pmb} is independent of optical thickness, approaching the line-of-sight distance (D_z) as the size of the square diminishes ($D_x \to 0$). In general, L_{pmb} decreases with optical thickness for a square with fixed dimension (D_x/D_z). Physically, this

behavior can be explained by noting that as the absorption coefficient increases, the region of the square away from the z-axis will have larger optical thickness and contributes less to the heat transfer, The radiative heat transfer is thus characterized by a smaller L_{pmb}. As the size of A_2 (D_x/D_z) increases, L_{pmb} approaches an asymptotic curve, independent D_x. This behavior can again be attributed to lower contribution to the total heat transfer from the optically thick outer portion of A_2, which also has a lower exchange factor. Indeed, he exchange factor, view factor and L_{pmb} thus all approach an asymptotic limit as the size of the absorbing area, A_2, increases.

Using the OPMBL, an approximation to the exchange factor can be written as

$$\left(\frac{ds_1 s_2}{dA_1}\right)_{approx.} = F_{d1-2} e^{-aL_{opmb}} \tag{14}$$

A comparison between Eq. (14) and the actual exchange factor is presented in Figure 6. The agreement is excellent. To further illustrate the error in using L_{opmb} to evaluate the exchange factor, a detailed comparison between the exact and approximate value of the exchange factor for a specific geometry ($\frac{D_x}{D_z} = \frac{D_y}{D_z} = 5$) is presented in Figure 7. Note that the absolute value of the error is less than 0.005 for all optical thicknesses. The maximum error occurs in the region around $aD_z \sim 0.3$, which yield a percentage error of about 2%. While the percentage error increases significantly in the region of large optical thickness ($aD_z > 2$), this error increase is not important since the value of the exchange factor is small (< 0.01) in this region. OPMBL can thus be used to predict accurately the exchange factor over all optical thicknesses. The OPMBL for A_2 with different dimensions (D_x/D_z, D_y/D_z) are presented in Figure 8. In general, OPMBL increases with increasing dimension in the x and y direction. In both direction, OPMBL approachs an asymptotic limit due to the decreasing contribution of radiative heat transfer from the outer portion of the absorbing surface.

A similar calculation is performed for the geometry as shown in Fig. (4b), in which A_2 is perpendicular to dA_1 with a dimension of $D_y \times D_z$ at the plane $x = D_x$. Based on the mathematical development presented in the appendix, the PMBL for this geometric configuration is given by

$$e^{-aL_{pmb}} = \frac{1}{\pi F_{d1-2}}\left[\int_0^{\eta_y} \frac{e^{-aD_x\sqrt{1+s^2}}}{(1+s^2)^2} s^2 ds + \eta_y \int_{\eta_y}^{\sqrt{\eta_y^2+\eta_z^2}} \frac{e^{-aD_x\sqrt{1+s^2}}}{(1+s^2)^2} s ds - \int_{\eta_z}^{\sqrt{\eta_y^2+\eta_z^2}} \frac{e^{-aD_x\sqrt{1+s^2}}}{(1+s^2)^2} \sqrt{s^2-\eta_z^2}\, s ds\right] \tag{15}$$

with $\eta_y = \frac{D_y}{D_x}$, $\eta_z = \frac{D_z}{D_x}$ and F_{d1-2} is the view factor given by

$$F_{d1-2} = \frac{1}{2\pi}\left[tan^{-1}\eta_y - \frac{1}{\sqrt{1+\eta_z^2}} tan^{-1}\left(\frac{\eta_y}{\sqrt{1+\eta_z^2}}\right)\right] \tag{16}$$

In general, the mathematical behavior of PMBL for the configuration in Fig. (4b) is similar to that of Fig (4a). The spectral dependence of PMBL, the existance of an OPMBL which can be used to accurately approximate the exchange factor over all values of the absorption coefficient, the small error of the approximation and overall behavior of the OPMBL are presented in Figs. (9), (10), (11) and (12) respectively.

4. Applications

To provide a quantitative assessment on how the concept of PMBL can improve the computational efficiency of a radiation solver, the OPMBL data generated for the geometric configurations of Fig. (4a) and (4b) (as represented by Figs. (8) and (12)) are implemented to evaluate the exchange factor between two finite rectangular areas oriented in the parallel and perpendicular direction as shown in Figs. (13a) and (13b). The total radiative exchange between the two finite surfaces is given by

$$s_1 s_2 = \int_0^\infty \int_{A_1} \int_{A_2} \frac{cos\theta_1 cos\theta_2}{\pi L^2} e^{-a_\lambda L} dA_2 dA_1 \, d\lambda \tag{17}$$

For a non-gray medium such as a mixture of combustion gas and soot, the spectral integration can be carried out to yield

$$s_1 s_2 = \int_{A_1} \int_{A_2} \frac{cos\theta_1 cos\theta_2}{\pi L^2} \tau_g(L) dA_2 dA_1 \tag{18}$$

Using the concept of OPMBL and the principle of superposition, the integration over A_2 can be written as a finite sum of differential exchange factors between dA_1 and finite rectangles with the geometry of Figs. (4a) and (4b) as

$$\int_{A_2} \frac{cos\theta_1 cos\theta_2}{\pi L^2} \tau_g(L) dA_2 = \sum_{i=1}^{N} F_{d1-2,i} \tau_g\left(L_{opmb,i}\right) \tag{18}$$

where the number of terms in the summation, N (which is less than or equal to 4), varies depending on the location of dA_1 relative to A_2. The total exchange factor is reduced to a single area integration over A_1 as

$$s_1 s_2 = \int_{A_1} \sum_{i=1}^{N} F_{d1-2,i} \tau_g\left(L_{pmb,av,i}\right) dA_1 \tag{19}$$

which can be evaluated efficiently.

Two specific cases are presented to illustrate the computational efficiency of the PMBL approach. In the first example, two parallel squares separated by a vertical distance equal to its width ($X_1 = Y_1 = 1$, $X_2 = Y_2 = 1$, $\Delta X = \Delta Y = 0$ and $\Delta Z = 1$ in Figure (13a) is considered. The neural network RADNNET [17], which has been established to be an accurate and efficient approach to determine the 1-D transmission characteristics of a CO_2/H_2O/soot mixture, is used to calculate the transmissivity. Results for some typical

values of H_2O partial pressure and soot concentration are presented in Table 1. The PMBL approach, based on Eq. (19), generates essentially the same value of the exchange factor as the direct integration approach based on Eq. (17) with a moderate reduction in computational effort (a factor of 3 to 4). Mathematically, the evaluation of exchange factor for parallel surfaces converges quickly even with a direct numerical approach. The improvement by the PMBL approach is thus not too significant.

In the second example, two perpendicular squares with a common edge ($X_1 = Y_1 = 1$, $Y_2 = Z_2 = 1$, $\Delta X = \Delta Y = \Delta Z = 0$ in Figure (13b) is considered. The evaluation of the exchange factor for this geometrical configuration by direct numerical integration is known to require significant effort because of the mathematical singularity associated with the common edge. This is confirmed by results shown in Table 2. The CPU time for an absorbing medium using the direct integration approach is in the range of 10 to 45 secs. The PMBL approach, on the other hand, is far superior. It yields results which are within 1% of the direct integration approach and the required computational effort (CPU time) is similar to that of the first example. Specifically, the required CPU time in this second example is in the range of 0.1 secs. or less, representing a factor of 100 to 400 reduction in computational effort. Mathematically, the direct integration approach needs a fine discretization in both A_1 and A_2 to account for the contribution of the region near the common edge to the exchange factor, leading to the excessive computational effort. The PMBL approach, on the other hand, requires only discretization of area A_1. Since PMBL approaches an asymptotic constant value as the integration point approaches the common edge, there is no need for very fine discretization. This accounts for the significant improvement in the required computational effort for the PMBL approach.

For the general geometry as shown in Figs. (13a) and (13b), two radiation solvers, RADNNET-SSPP-MBL and RADNNET-SSPD-MBL are developed using the PMBL approach. Since they are computationally efficient, these two solvers can be used in a time-transient calculation for practical engineering applications. They can also be used to generate much needed benchmark solutions for the further development of computational method for radiative heat transfer. These solvers are made available for the engineering community from the websites walter-yuen.com/radnnet-sspp-mbl and walter-yuen.com/radnnet-sspd-mbl respectively.

5. Conclusion

A new concept of point mean beam length (PMBL) is presented. For a specific geometry, a constant "optimal" point mean beam length is shown to be sufficient to simulate the non-gray effect of radiative heat transfer. For enclosures with symmetrical geometry, PMBL is identical to the traditional mean beam length concept. It provides a mathematical justification for the current empirical approach for the utilization of the mean beam length concept for practical application. For radiative heat transfer in general multi-dimensional enclosure, PMBL is shown to be highly effective in improving the computational efficiency of radiative heat transfer in multi-dimensional non-gray media. As illustrations, two radiation solvers using the PMBL are developed and made available to the engineering community.

6. References

1. H. C. Hottel and A. F. Sarofim, "Radiative Transfer," McGraw Hill, New York, 1967.
2. R. V. Dunkle, "Geometric Mean Beam Length for Radiant Heat Transfer Calculations", ASME Journal of Heat Transfer, Vol. 86, No. 1, pp. 75-80, 1964.
3. D. B. Olfe, "Mean Beam Length Calculations for Radiation from Non-Transparent Gases", Journal of Quantitative Spectroscopy and Radiative Transfer, Vol. 1, pp. 169-176, 1961.
4. C. L. Tien and L. S. Wang, "On the Calculation of Mean Beam Length for a Radiating Gas," Journal of Quantitative Spectroscopy and Radiative Heat Transfer, Vol. 5, pp. 453-456, 1965.
5. A. T. Wassel and D. K. Edwards, "Mean Beam Length for Spheres and Cylinders," ASME Journal of Heat Transfer, Vol. 98, pp. 308-309, 1976.
6. D. A. Mandell, "Exact and Mean Beam Length Calculations for Radiative Heat Transfer in Gases," Combustion Science and Technology, Vol. 9, pp. 273-276, 1974.
7. D. A. Nelson, "Band Radiation of Isothermal Gases with Diffused Wall Enclosures", International Journal of Heat and Mass Transfer, Vol. 27, No. 10, pp. 1759-1769, 1984.
8. W. W. Yuen, "A Simplified Approach to the Evaluation of Geometric Mean Transmittance and Absorptance for Gas Enclosures," ASME Journal of Heat Transfer, Vol. 103, pp. 808-813, November, 1981.
9. W. W. Yuen, "Evaluation of Geometric Mean Transmittance and Total Absorptance for Two-Dimensional Systems," International Journal of Heat and Mass Transfer, Vol. 25, No. 7, pp. 1069-1071, 1982.
10. W. W. Yuen, "Definition and Evaluation of Mean Beam Length for Applications in Multi-Dimensional Radiative Heat Transfer, a Mathematically Self-Consistent Approach", ASME Journal of Heat Transfer, Vol. 130, pp. 114507-1-5, Nov. 2008.
11. W. W. Yuen, "On the Utilization of the Mean Beam Length Concept in the Evaluation of Radiative Heat Transfer in Isothermal Three-Dimensional Non-Gray Systems", International Journal of Heat and Mass Transfer, Vol. 84, pp. pp. 809-820, 2015.
12. R. Siegel and J. Howell, "Thermal Radiation Heat Transfer", 4th Ed., Taylor and Francis, New York, 2002.
13. W. C. Tam, "Analysis of Heat Transfer in a Building Structure Accounting for the Realistic Effect of Thermal Radiation Heat Transfer," Ph.D. Thesis, The Hong Kong Polytechnic University (2013).
14. W. W. Jones, R. D. Peacock, G. P. Forney and P. A. Reneke, "CFAST: Consolidated Model of Fire Growth and Smoke Transport (Version 5), Technical Reference Guide," NIST-SP-1030, National Institute of Standard and Technology, October, 2004.
15. K. McGrattan, S. Hostikka, J. Floyd, H. Baum. and R. Rehm, "Fire Dynamics Simulator (Version 5), Technical Reference Guide," NIST Special Publication 1018-5, National Institute of Standard and Technology, October 1, 2007.
16. Yuen, W. W., "RAD-NNET, a Neural Network Based Correlation Developed for a Realistic Simulation of the Non-gray Radiative Heat Transfer Effect in Three-dimensional Gas-particle Mixtures." *International Journal of Heat and Mass Transfer*, 52, 3159–3168 (2009).

7. Appendix

For the geometry as shown in Fig. (4a), the exchange factor between dA_1 and A_2 is given by

$$\frac{ds_1 s_2}{dA_1} = \frac{1}{\pi}\iint \frac{e^{-ar}D_z^2}{r^4} dA_2 \tag{A1}$$

with $r = \sqrt{x^2 + y^2 + D_z^2}$ $\quad dA_2 = dxdy$. In terms of a polar coordinate on the x-y plane ($dA_2 = sdsd\phi$), Eq. (A1) can be written as

$$\begin{aligned}\frac{ds_1 s_2}{dA_1} &= \int_0^{\sqrt{D_x^2+D_y^2}} \int_{\phi_{min}(s)}^{\phi_{max}(s)} \frac{e^{-ar}D_z^2}{\pi r^4} sdsd\phi \\ &= \int_0^{\sqrt{D_x^2+D_y^2}} [\phi_{max}(s) - \phi_{min}(s)] \frac{e^{-ar}D_z^2}{\pi r^4} sds\end{aligned} \tag{A2}$$

with $s = \sqrt{x^2 + y^2}$. The two angular limit of integration, $\phi_{min}(s)$ and $\phi_{max}(s)$ for three separate range of s can be determined geometrical as shown in Fig. (A1). Eq. (A2) is reduced to three separate terms as follow

$$\begin{aligned}\frac{ds_1 s_2}{dA_1} &= \frac{1}{2}\int_0^{D_x} \frac{e^{-ar}D_z^2}{r^4} sds + \frac{1}{\pi}\int_{D_x}^{D_y} \left[\frac{\pi}{2} - cos^{-1}\left(\frac{D_x}{s}\right)\right] \frac{e^{-ar}D_z^2}{r^4} sds + \\ &\frac{1}{\pi}\int_{D_y}^{\sqrt{D_x^2+D_y^2}} \left[sin^{-1}\left(\frac{D_y}{s}\right) - cos^{-1}\left(\frac{D_x}{s}\right)\right] \frac{e^{-ar}D_z^2}{r^4} sds\end{aligned} \tag{A3}$$

Eq. (A3) can be further simplified to yield

$$\begin{aligned}\frac{ds_1 s_2}{dA_1} &= \frac{1}{2}\left[E_3(aD_z) - \left(\frac{1}{\sqrt{\zeta_y^2+1}}\right)^2 E_3\left(aD_z\sqrt{\zeta_y^2+1}\right)\right] \\ &-\frac{1}{\pi}\int_{\zeta_x}^{\sqrt{\zeta_x^2+\zeta_y^2}} cos^{-1}\left(\frac{\zeta_x}{s}\right)\frac{e^{-aD_z r}}{r^4} sds + \frac{1}{\pi}\int_{\zeta_y}^{\sqrt{\zeta_x^2+\zeta_y^2}} sin^{-1}\left(\frac{\zeta_y}{s}\right)\frac{e^{-aD_z r}}{r^4} sds\end{aligned} \tag{A4}$$

which is the basis of Eq. (12). Note that even though the identification of the angular limits of integration, as shown in Fig. (A1) is based on the assmuption of $D_x < D_y$, Eq. (A4) is general and applicable for all values of (D_x, D_y). In the optically thin limit ($aD_z \to 0$), Eq. (A4) can be integrated to yield the view factor expression shown in Eq. (13).

For the configuration of Fig. (4b), the exchange factor is given by

$$\frac{ds_1 s_2}{dA_1} = \frac{1}{\pi}\iint \frac{e^{-ar}D_x z}{r^4} dA_2 \tag{A5}$$

with $r = \sqrt{D_x^2 + y^2 + z^2 +}$ $\quad dA_2 = dydz$. Similar to Eq. (A2), Eq. (A5) is expressed In terms of a polar coordinate on the y-z plane ($dA_2 = sdsd\phi$) as

$$\frac{ds_1 s_2}{dA_1} = \int_0^{\sqrt{D_y^2+D_z^2}} \int_{\phi_{min}(s)}^{\phi_{max}(s)} \frac{e^{-ar_{D_x}} scos\phi}{\pi r^4} sdsd\phi$$
$$= \int_0^{\sqrt{D_y^2+D_z^2}} \left[\sin\left(\phi_{max}(s)\right) - sin\left(\phi_{min}(s)\right)\right] \frac{e^{-ar_{D_x}}}{\pi r^4} s^2 ds \qquad \text{(A6)}$$

with $s = \sqrt{y^2 + z^2}$. The angular limits of the integration is similar to those presented in Fig. (A1) with the substitution of $D_x \to D_z$. Eq. (A6) is reduced to three separate integrals as

$$\frac{ds_1 s_2}{dA_1} = \int_0^{D_y} \frac{e^{-ar_{D_x}}}{\pi r^4} s^2 ds - \int_{D_z}^{\sqrt{D_y^2+D_z^2}} \frac{e^{-ar_{D_x}}}{\pi r^4} \sqrt{1 - \frac{D_z^2}{s^2}} s^2 ds + \int_{D_y}^{\sqrt{D_y^2+D_z^2}} \frac{e^{-ar_{D_x}}}{\pi r^4} sD_y ds \quad \text{(A7)}$$

After non-dimensionalization, Eq. (A7) is reduced to

$$\frac{ds_1 s_2}{dA_1} = \frac{1}{\pi} \int_0^{\eta_y} \frac{e^{-aD_x\sqrt{1+s^2}}}{(1+s^2)^2} s^2 ds + \frac{\eta_y}{\pi} \int_{\eta_y}^{\sqrt{\eta_y^2+\eta_z^2}} \frac{e^{-aD_x\sqrt{1+s^2}}}{(1+s^2)^2} sds -$$
$$\frac{1}{\pi} \int_{\eta_z}^{\sqrt{\eta_y^2+\eta_z^2}} \frac{e^{-aD_x\sqrt{1+s^2}}}{(1+s^2)^2} \sqrt{s^2 - \eta_z^2} sds \qquad \text{(A8)}$$

which is the basis of Eq. (15). Similar to Eq. (A4), Eq. (A8) is general and applicable for all values of (D_y, D_z). In the optically thin limit ($aD_x \to 0$), Eq. (A8) can be integrated to yield the view factor expression shown in Eq. (16).

Case	$T_g = T_w$ (K)	p_{H_2O} (kPa)	f_v	$s_1 s_2$ (Eq. 17)	CPU (sec)	$s_1 s_2$(PMBL) (Eq. 19)	CPU (PMBL) (sec)
1	1000	0	0	0.1998	1.563E-2	0.1998	1.563E-2
2	1000	0	5E-8	0.1805	3.125E-2	0.1805	3.125E-2
3	1000	0	1E-7	0.1635	4.688E-2	0.1634	1.563E-2
4	1000	30	0	0.1404	1.047	0.1404	0.2500
5	1000	30	5E-8	0.1257	0.8125	0.1257	0.2500
6	1000	30	1E-7	0.1130	0.6719	0.1130	0.2500

Table 1: Comparison of the CPU time requirements for the evaluation of the exchange factor between two parallel squares with a vertical separation equal to its width ($X_1 = Y_1 = 1$, $X_2 = Y_2 = 1$, $\Delta X = \Delta Y = 0$ and $\Delta Z = 1$ in Figure 10a).

Case	$T_g = T_w$ (K)	p_{H_2O} (kPa)	f_v	$s_1 s_2$ (Eq. 17)	CPU (sec)	$s_1 s_2$(PMBL) (Eq. 19)	CPU (PMBL) (sec)
1	1000	0	0	0.2000	1.563E-2	0.2000	1.563E-2
2	1000	0	5E-8	0.1901	3.125E-2	0.1909	1.563E-2
3	1000	0	1E-7	0.1811	1.562E-2	0.1824	1.563E-2
4	1000	30	0	0.1615	45.95	0.1630	0.1563
5	1000	30	5E-8	0.1537	10.78	0.1556	0.1250
6	1000	30	1E-7	0.1465	10.51	0.1487	0.1094

Table 2: Comparison of the CPU time requirements for the evaluation of the exchange factor between two perpendicular squares with a common edge ($X_1 = Y_1 = 1$, $Y_2 = Z_2 = 1$, $\Delta X = \Delta Y = \Delta Z = 0$ in Figure 10b).

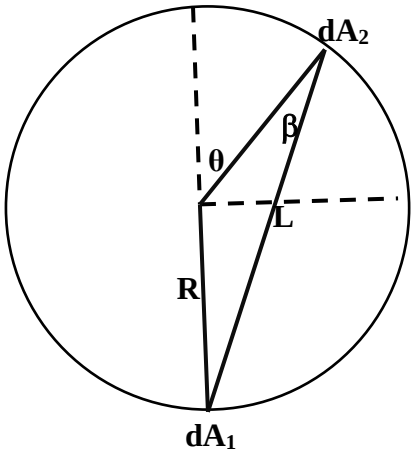

Figure 1: Geometry and coordinate system for a spherical system.

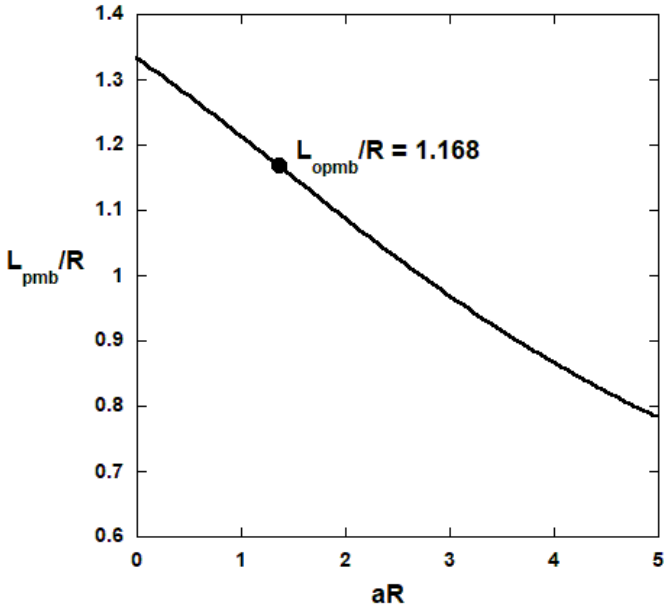

Figure 2: The effective of optical thickness (*aR*) on PMBL for a spherical enclosure and the value of OPMBL.

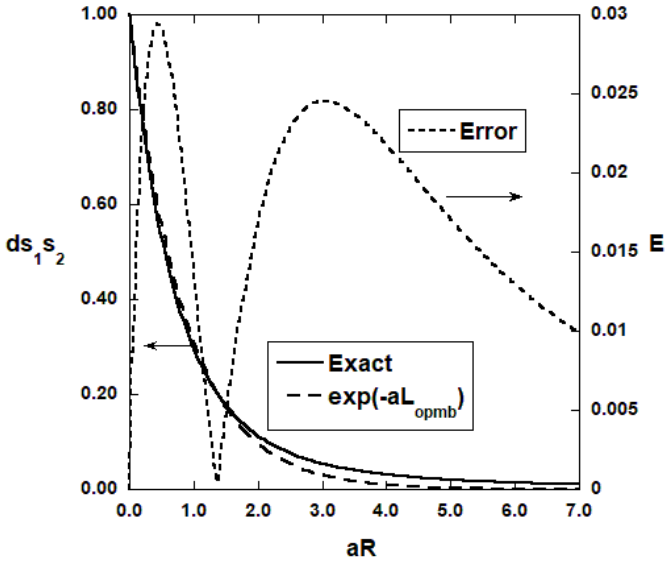

Figure 3: Comparison between the exact and approximate exchange factor generated by OPMBL and the error of the approximation.

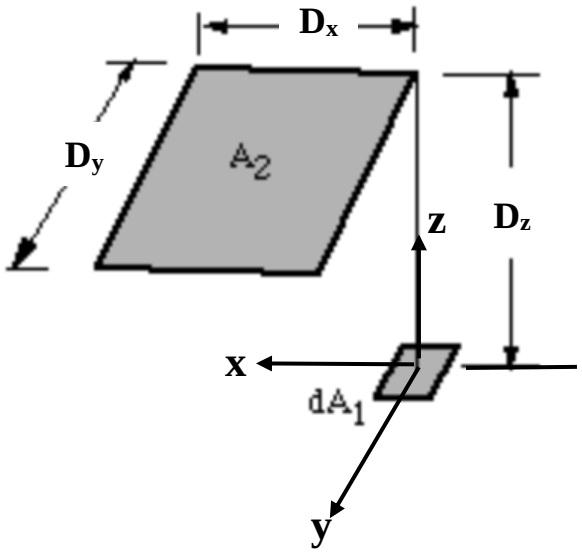

Figure 4a: Geometry and coordinate system of the first 3-D fundamental geometry.

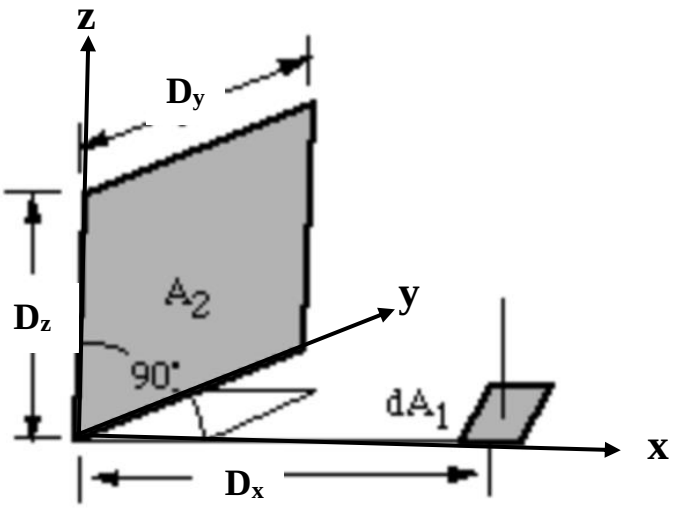

Figure 4b: Geometry and coordinate system of the second 3-D fundamental geometry

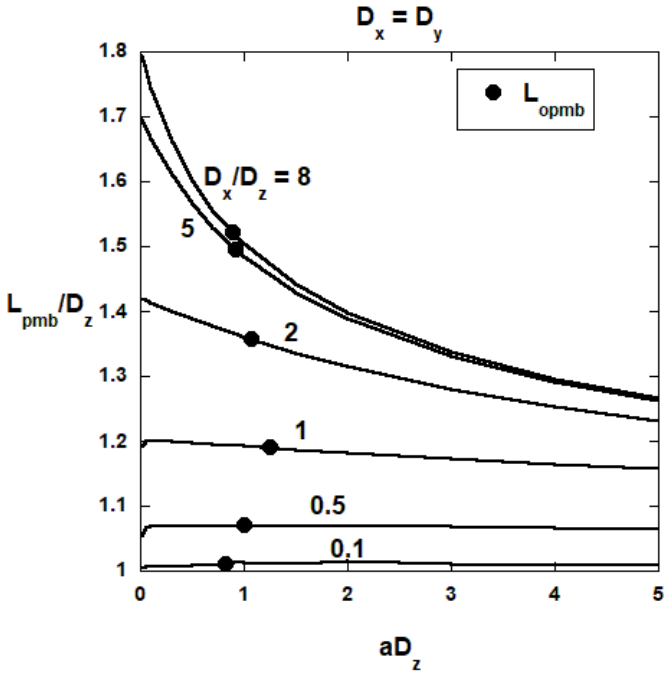

Figure 5: The effect of optical thickness (aD_z) and physical dimension (D_x/D_z) on PMBL for the configuration of Fig. 4a.

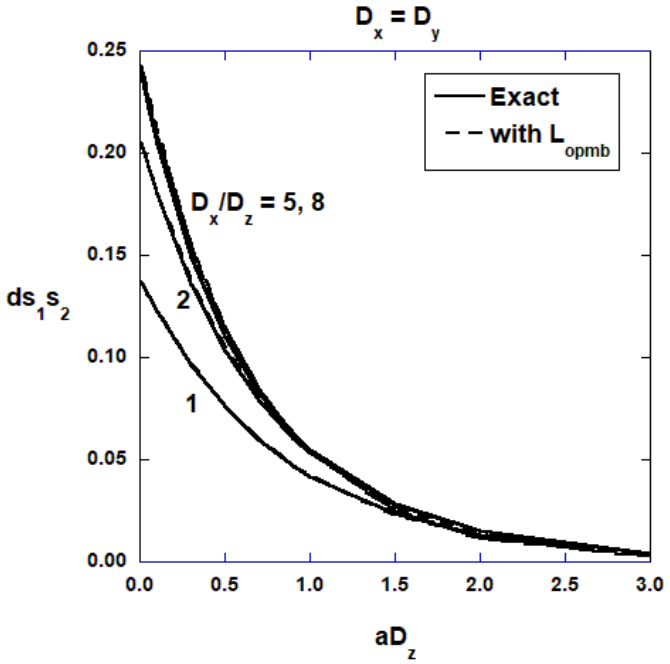

Figure 6: Comparison between the exact value of the exchange factor and the approximation using PMBL for the configuration of Fig. 4a.

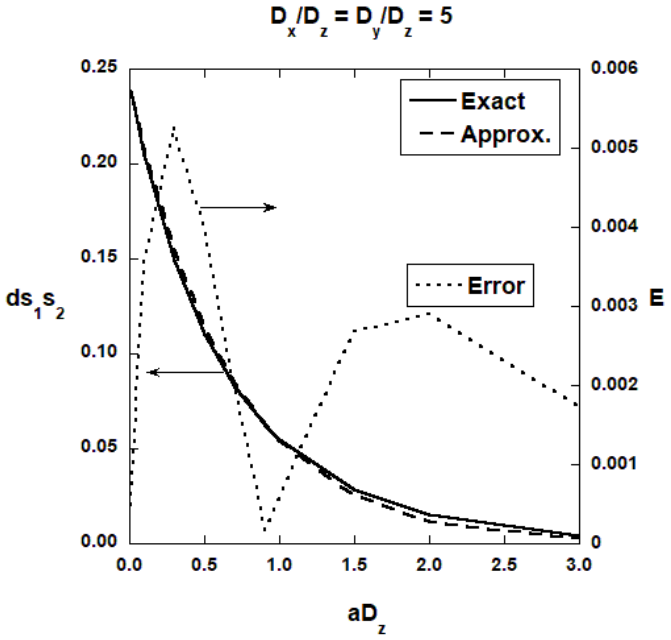

Figure 7: Comparison between the exact and approximate exchange factor generated by the OPMBL and the error of the approximation for the case with $D_x/D_z = D_y/D_z = 5$.

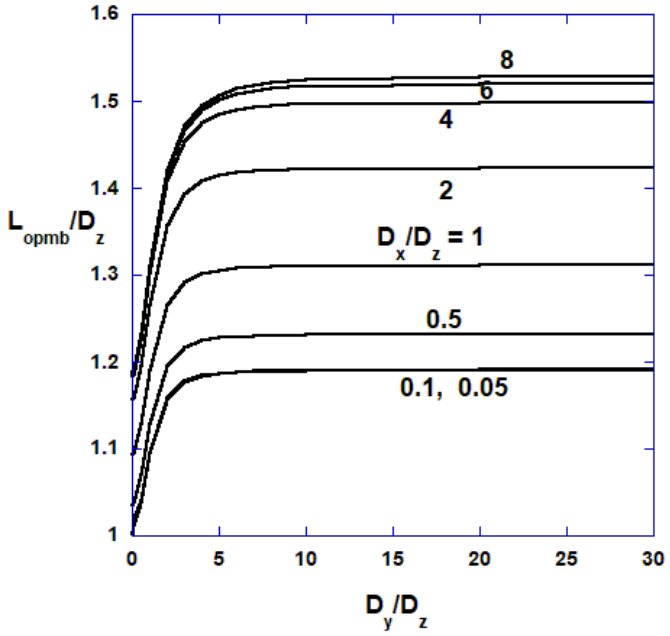

Figure 8: OPMBL for different dimensions of A_2 for the configuration of Fig. 4a.

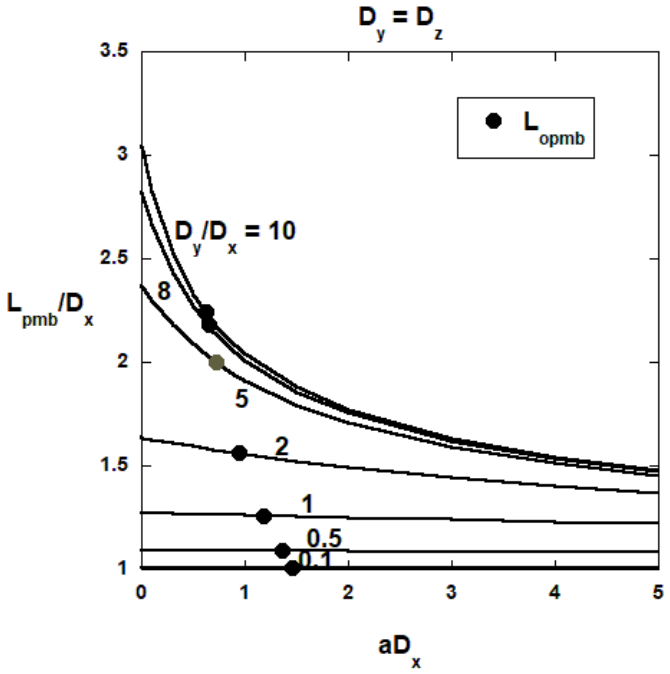

Figure 9: The effect of optical thickness (aD_z) and physical dimension (D_x/D_z) on PMBL for the configuration of Fig. 4b.

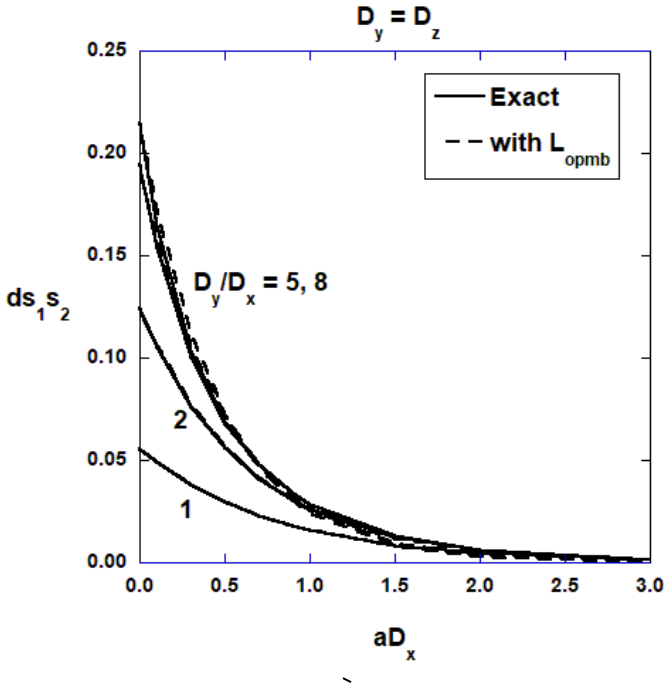

Figure 10: Comparison between the exact value of the exchange factor and the approximation using PMBL for the configuration of Fig. 4b.

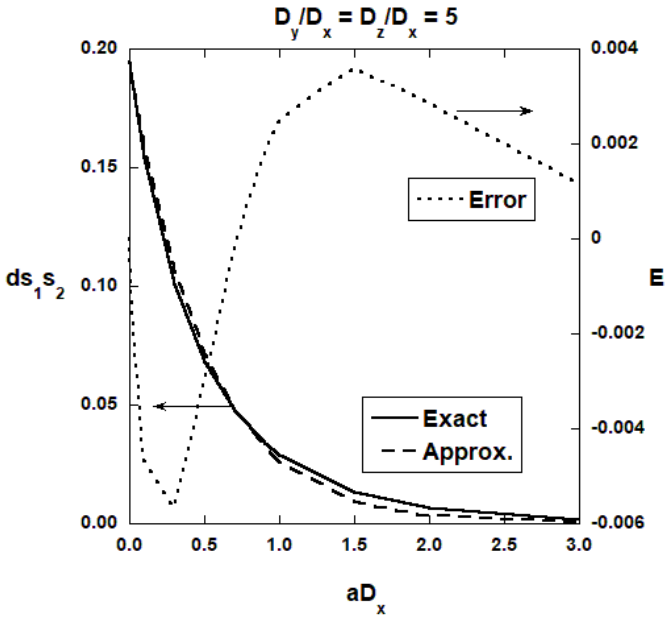

Figure 11: Comparison between the exact and approximate exchange factor generated by OPMBL and the error of the approximation for the case with $D_z/D_x = D_y/D_x = 5$.

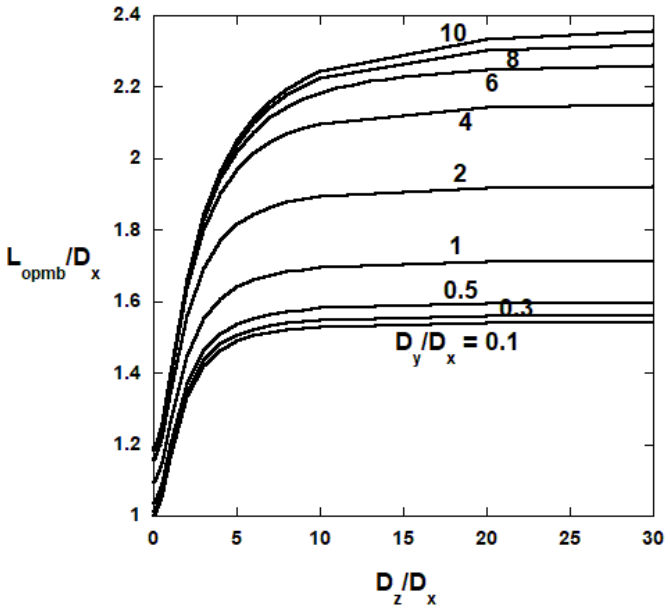

Figure 12: OPMBL for different dimensions of A_2 for the configuration of Fig. 4b.

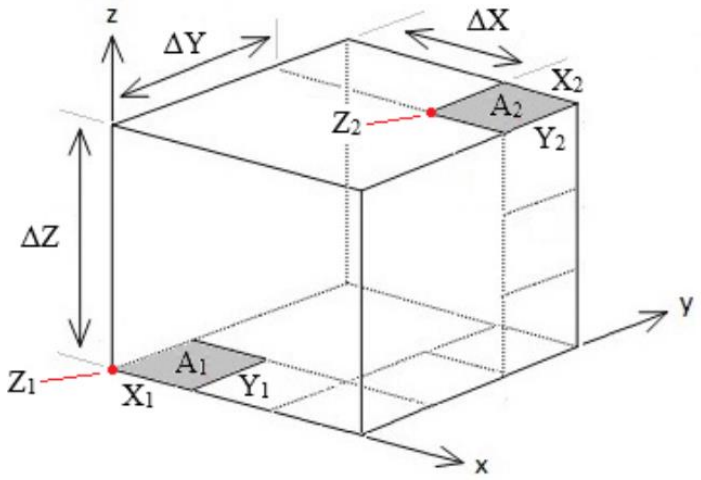

Figure 13a: Geometry and coordinate System for SSPP, the evaluation of exchange factor between two parallel rectangles.

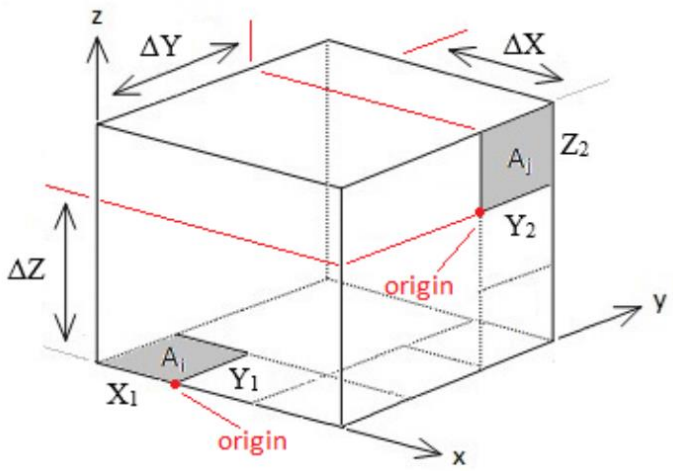

Figure 13b: Geometry and coordinate system for SSPD, the evaluation of exchange factor between two perpendicular rectangles.

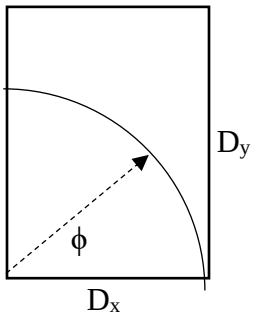

For $s < D_x$, $\phi_{min} = 0$, $\phi_{max} = \frac{\pi}{2}$

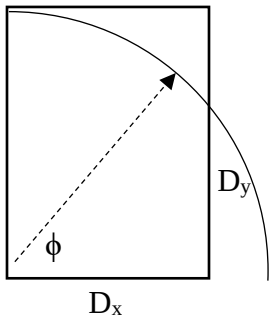

For $D_x < s < D_y$,
$\phi_{min} = cos^{-1}\left(\frac{D_x}{s}\right)$, $\phi_{max} = \frac{\pi}{2}$

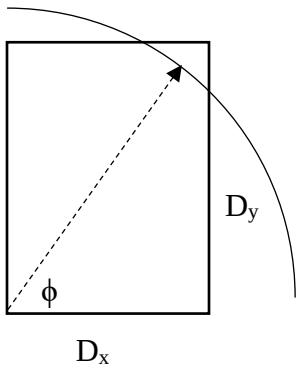

For $D_y < s < \sqrt{D_x^2 + D_y^2}$,
$\phi_{min} = cos^{-1}\left(\frac{D_x}{s}\right)$, $\phi_{max} = sin^{-1}\left(\frac{D_y}{s}\right)$

Figure A1: Angular limits for the integration in Eq. (A2).